Anisotropic Propagation and Damping of Spin Waves in a Nanopatterned Antidot Lattice

S. Neusser,[1] G. Duerr,[1] H. G. Bauer,[2] S. Tacchi,[3] M. Madami,[3] G. Woltersdorf,[2] G. Gubbiotti,[3] C. H. Back,[2] and D. Grundler[1,*]

[1]*Lehrstuhl für Physik funktionaler Schichtsysteme, Technische Universität München, Physik Department, James-Franck-Str. 1, D-85747 Garching b. München, Germany*
[2]*Institut für Experimentelle und Angewandte Physik, Universität Regensburg, D-93040 Regensburg, Germany*
[3]*CNISM, Dipartimento di Fisica, Universita di Perugia, Via A. Pascoli, I-06123 Perugia, Italy*
(Received 1 June 2010; revised manuscript received 8 July 2010; published 6 August 2010)

All-electrical spin-wave spectroscopy, Brillouin light scattering, as well as the magneto-optical Kerr effect are combined to study spin-wave propagation through a magnetic antidot lattice nanopatterned into a $Ni_{80}Fe_{20}$ thin film. The propagation velocities and, in particular, the relaxation are found to depend characteristically on the applied in-plane magnetic field. We explain the observed anisotropies by magnetic field-controlled spin-wave guiding in a network of interconnected nanowires which takes place over distances of up to 20 μm.

PACS numbers: 75.40.Gb, 75.30.Ds, 75.75.−c, 75.78.−n

Spin excitations in periodically nanostructured ferromagnets have generated considerable interest recently in view of spin-wave (SW) filters [1] and magnonic crystals [2–4], i.e., the magnetic counterpart of a photonic crystal. Experimental and theoretical studies on these subjects have fueled the research field of magnonics [5–7]. As promising magnetic devices, antidot lattices consisting of a periodic array of nanopatterned holes in a ferromagnetic film have been considered, e.g., for field-controlled SW guiding [5]. Spin-wave propagation has recently been investigated in plain films [8–12] and individual magnetic wires [13–15] using different techniques such as Brillouin light scattering (BLS), all-electrical spin-wave spectroscopy (AESWS), and time-resolved magneto-optical Kerr microscopy (TR-MOKE). Detailed investigations on SW propagation velocities and corresponding damping characteristics in nanostructures are however missing. In particular the antidot lattice, if considered as a two-dimensional network of interconnected magnetic nanowires, is a relevant model system to study the possible anisotropy effects of SW propagation. A deep understanding of the respective parameters is of utmost importance for fundamental research and envisioned applications. We combine BLS, AESWS, and TR-MOKE measurements to develop a thorough understanding. Micromagnetic simulations are used to further interpret the data. The findings are also relevant for the development of, both, spin-wave filters and magnonic crystals.

For the experiments, two open-ended coplanar wave guides (CPWs) were integrated on top of a $Ni_{80}Fe_{20}$ (permalloy) film of nominal thickness $b = 22$ nm [Fig. 1(a)]. The saturation magnetization was $M_s \approx 760$ kA/m as measured via ferromagnetic resonance [16]. The permalloy film was periodically patterned into a square lattice with holes of diameter $\delta = 120$ nm $\pm$ 30 nm forming an antidot array. The primitive lattice vectors of the antidot lattice were collinear with the CPWs [Fig. 1(a)]. Different lattice

constants were fabricated ranging from $d = 400$ to 1000 nm using focussed ion beam etching. In this Letter we focus on data obtained on $d = 800$ nm. This corresponded to a $Ni_{80}Fe_{20}$ filling fraction of 93%. The further arrays support the findings presented here. The magnetic film was capped with a thin insulating layer of SiO_2. The two CPWs were connected to the source and detector of a vector network analyzer to perform AESWS. They acted as
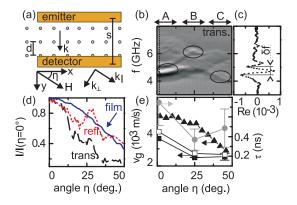

FIG. 1 (color online). (a) Sketch of the sample. Two CPWs labeled emitter and detector are integrated with an antidot lattice. The holes (diameter of 120 nm) are arranged on a square lattice with a period $d = 800$ nm. The wave vector k transferred by the CPW is orientated in the y direction. (b) All-electrical spectroscopy data ReS_{21} in transmission configuration for different η ($\mu_0H = 20$ mT). The propagation length was $s = 6.5$ μm. Three relevant regimes A, B, and C are highlighted. (c) Single spectrum ReS_{21} taken at $\eta = 2°$. (d) Relative variation of intensities measured in reflection (dotted line) and transmission (dashed line) configuration ($s = 12$ μm). The full line shows data obtained on a plain film in transmission. (e) Group velocities v_g obtained in regimes A, B, and C. Full black (open white) squares denote v_g obtained through AESWS (BLS). Full triangles show v_g from a plain film. Full circles represent the effective relaxation time τ for propagating SWs.

a SW emitter and detector, respectively. The source supplied a continuous-wave sinusoidal radio-frequency (rf) current exciting spin precession underneath the emitter CPW [16]. We measured in reflection and transmission configuration, by which we studied local SW excitation and SW propagation, respectively. We measured the real part Re and the amplitude I of the voltage signals. In the transmission configuration the signals contained more information than the local rf susceptibility only [16]. The vector network analyzer detected in particular phase sensitively the spin precession at the detector CPW. This was the necessary requirement to extract SW propagation velocities v_g. The CPW excited a broad spectrum of wave vectors in the y direction with values of up to π/w, where w was the width of the inner conductor [8,17]. The maximum of the excitation was around $k_y \approx \pi/(2w)$. In order to minimize the electromagnetic (em) coupling and optimize the SW signals, antidot lattices with CPWs of different w and propagation distances s were fabricated and tested. The smallest width $w = 800$ nm ($s = 6.5$ μm) generated SWs around $k_y = 1.9 \times 10^4$ rad/cm. Other designs had $s = 12.5$ μm ($w = 2$ μm) and $s = 19.5$ μm ($w = 4$ μm). By changing s the spin-wave phase delay between emitter and detector CPWs was varied entering the voltage signal. The sample was placed in an external field **H** applied under an angle η with respect to the CPWs. In Fig. 1(a) we subdivide the SW wave vector **k** into two components parallel ($k_\parallel$) and perpendicular ($k_\perp$) to **H** considering $k^2 = k_\parallel^2 + k_\perp^2$ [18]. A reference technique was used in order to increase the signal-to-noise ratio in AESWS by subtracting the spectrum obtained for $\mu_0 H = 100$ mT and $\eta = 90°$ [19]. For TR-MOKE microscopy of the spin-precession amplitudes the detector CPW on a nominally identical antidot lattice was omitted and the optical probe pulses were phase locked to the microwave generator. The spatial resolution was about 250 nm [20]. To explore SW propagation characteristics for a broader range of wave vectors we employed BLS where light was inelastically scattered from thermally excited spin waves [3]. By changing the incidence angle of the light, we varied both the direction of **k** and the in-plane component of k entering into the scattering process.

First, AESWS data shown in Fig. 1(b) is discussed where a CPW with inner conductor width $w = 0.8$ μm has been used. Here the real part of the transmitted signal Re(S_{12}) is plotted. Near specific spin-wave resonances, the contrast in the gray-scale plot oscillates between white and black as a function of frequency f at fixed η with a period δf as defined in Fig. 1(c). Such oscillations are highlighted by circles in Fig. 1(b) and indicate SW propagation as will be discussed later. It is interesting that in the angular regimes labeled A and C, SW propagation is observed between 4 and 5 GHz whereas in regime B this occurs at higher frequencies of about 6 to 7 GHz. In regime B, a further low-frequency mode without contrast oscillation is visible. Amplitudes I, which have been measured on a

sample with $s = 12.5$ μm, are shown in Fig. 1(d). Thereby we have minimized the em coupling and extracted reliable values of I. In the transmission configuration (dashed line) I decreases strongly with increasing η, recovers around $\eta = 25°$, and reaches a minimal value already for $\eta \gtrsim 30°$. This is not observed for an unpatterned reference film where the transmitted signal I exhibits a smooth decay (full line). The smooth decay can be explained by two effects. First, with increasing η, v_g decreases due to the transition from Damon-Eshbach modes where **k** $\perp$ **M** towards backward volume modes where **k** $\parallel$ **M**. Secondly, the excitation (detection) strength underneath the CPW decreases with increasing η due to a decreasing torque exerted by the rf field onto the magnetization. To exclude angle-dependent excitation conditions as the reason for the pronounced decrease of I in the antidot lattice, we show data obtained in reflection configuration as well (dotted line). It shows a characteristic angular dependence but a less pronounced reduction with η. The purpose of this Letter is to explain the microscopic origin of the striking differences in the angle-dependent amplitudes I.

In the following we interpret the contrast oscillations in Fig. 1. It has already been reported that an otherwise Lorentzian-shaped SW rf susceptibility splits up in a multipeak structure in AESWS if SW propagation occurs between emitter and detector CPWs [8]. The period δf is a measure of the phase difference $\delta\phi$ which spin waves of different eigenfrequencies experienced along the propagation path. δf corresponds to a change $\delta\phi = 2\pi$ of the spin waves' phases [8,15] and, obviously, a change $\delta k = \delta\phi/s = 2\pi/s$ of the wave vectors. One extracts the corresponding group velocity v_g according to

$$v_g = \frac{\partial\omega}{\partial k} \approx \frac{2\pi\delta f}{2\pi/s} = \delta f s. \qquad (1)$$

In our experiment a large number of oscillations is observed when using a small w. Precise values of v_g [black squares in Fig. 1(e)] have been extracted by using Eq. (1) for $w = 0.8$ μm (propagation distance $s = 6.5$ μm). We find $v_g = 3.6 \times 10^3$ m/s in regime A and $v_g = 2.5 \times 10^3$ m/s in regimes B and C. For small angles, the group velocities in the antidot lattice are considerably smaller than the values obtained on a plain film [full triangles in Fig. 1(e)]. The angular dependent change of the propagation velocities v_g is more pronounced than in the plain film. It is, furthermore, larger than expected from corresponding dispersion relations taking into account the frequency differences between modes A, B, and C. Remarkably, near $\eta = 45°$, SWs experience the same velocity of about $v_g = 2.5 \times 10^3$ m/s in both the antidot lattice and film.

Before analyzing the data of Fig. 1 in further detail, TR-MOKE data measured on the antidot lattice in regimes A, B, and C [upper row in Figs. 2(a)–2(c)] are presented. In the lower row of Figs. 2(a)–2(c) local spin-precession amplitudes are displayed which are obtained from micromagnetic simulations. Bright colors denote

large spin-precession amplitudes [21,22]. We note that micromagnetic simulations are performed at $k = 0$ and therefore the simulated eigenfrequencies are smaller than the experimental values extracted from the AESWS data in Fig. 1 (b). In the latter case we have $k = 1.9 \times 10^4$ rad/cm. The simulated frequencies agree well with BLS data at $k = 0$ [cf. Fig. 3]. A good one-to-one correspondence between the TR-MOKE data and simulated profiles is found. We emphasize that for $\mu_0 H > 15$ mT these profiles do not change significantly with increasing H. This allowed us to obtain best quality MOKE data at fields larger than $\mu_0 H = 20$ mT resulting in eigenfrequencies which differ from the simulated values. For regimes A and C stripelike regions of large spin-precession amplitude are observed which extend through the lattice. Their effective width is determined to be about 600 nm and 600 nm/$\sqrt{2}$, respectively. The stripes are oriented perpendicular to the applied field **H**. In regime B the profile of the propagating mode is found to be complex and significantly different from A and C. The mode shows an extended character in the y direction but localization between next-nearest neighboring holes.

The orientation of the stripelike spin-precession profile found in regime C is diagonal with respect to the primitive lattice vectors of the antidot array. The wave vector transferred by the CPW is orientated along the y direction and thus misaligned with respect to the longitudinal direction of these stripes by 45°. To explore the impact of this misalignment on the propagation characteristics, we perform BLS in three different scattering configurations [cf. insets in Figs. 3(a)–3(c)]. Here **k** is always perpendicular to **H** and collinear with the stripes in regimes A and C in Fig. 2(a). In Fig. 3(a) (regime A) one finds two nearly dispersionless modes (open circles) at high frequencies and

one branch with positive dispersion (full circles) which starts at 4 GHz at $k = 0$. From this one extracts a group velocity of $v_g = 4.0 \times 10^3$ m/s consistent with the AESWS data. The ansatz of Ref. [18] allows us to remodel the branch with positive dispersion [full line in Fig. 3(a)] by considering the component $k_\parallel$ to be quantized to a value of $k_\parallel = \pi/600$ nm. The quantization reflects the effective stripe width as determined from Fig. 2(a). The dispersion as a function of $k_\perp$ is calculated using Ref. [24] and found to be in good agreement with the measured data. In Fig. 3(b) dispersionless modes are observed at low frequency and a dispersive mode with $v_g = 2.7 \times 10^3$ m/s only at high frequency. This is in agreement with regime B of Fig. 1(b). In Fig. 3(c) again the low-frequency excitations exhibit $v_g > 0$. If compared to regime A, the stripes of regime C have a smaller width of 600 nm/$\sqrt{2}$. A dispersion calculated with $k_\parallel = \pi/(600$ nm/$\sqrt{2})$ (full line) is consistent with the AESWS data. We extract $v_g = 2.7 \times 10^3$ m/s from the BLS data. Consequently one concludes that in AESWS propagation for $\eta = 45°$ occurs along diagonal stripes through the antidot lattice such as those depicted in Fig. 2(c). As a result, a Damon-Eshbach mode, quantized in the transverse direction, is formed. The corresponding group velocity is comparable to the plain film mode with $\sphericalangle(\mathbf{k}, \mathbf{H}) = 45°$. Obviously the propagation path in the lattice between emitter and detector CPW is increased to $\sqrt{2}s$ which we have already considered when calculating the group velocity from AESWS data. Because of the complex and fully two-dimensional spatial SW profile, the dispersion of mode B [Fig. 2(b)] cannot be calculated using existing theories.

In the following effective relaxation times τ for the different propagating modes are determined according to $\frac{I}{I_0} = \exp(\frac{-t}{\tau})$ by AESWS. The parameter τ describes how the SW amplitude I depends on the propagation time t. I_0 is the amplitude at minimum delay time. Using a pulsed excitation for time-resolved signal detection has proven difficult for the direct determination of τ due to the super-
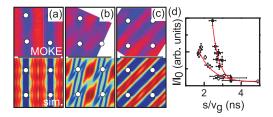

FIG. 2 (color online). (a)–(c) Spatial spin-wave mode profiles obtained by TR-MOKE (upper row). Shown are modes in the three regimes A, B, and C which are found to propagate away from the emitter CPW. Data are taken at (a) $f = 8$ GHz ($\eta = 0°$, $\mu_0 H = 68$ mT), (b) $f = 5.2$ GHz ($\eta = 25°$, $\mu_0 H = 20$ mT), and (c) $f = 8$ GHz ($\eta = 30°$, $\mu_0 H = 75$ mT). A nominally 28 nm thick permalloy film has been used to increase the signal-to-noise ratio. Simulation data (lower row) are obtained at $\mu_0 H = 20$ mT and, in particular, $k = 0$. The eigenfrequencies are (a) 3.8, (b) 4.3, and (c) 3.9 GHz. Bright (dark) contrast reflects high (low) spin-precession amplitude. (d) AESWS amplitude I/I_0 at the detector CPW as a function of $t = s/v_g$ for $\eta = 0°$ (white squares) and 25° (black squares). v_g is varied by changing $\mu_0 H$ from 15 to 60 mT. We use a sample with $w = 0.8$ μm and $s = 6.5$ μm. Full lines reflect Eq. (2).
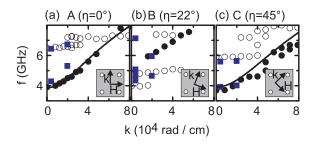

FIG. 3 (color online). Spin-wave dispersions for regimes A (a), B (b), and C (c) as obtained by BLS (circles) at $\mu_0 H = 20$ mT. Full (open) circles highlight the propagating (standing) wave character of different modes. Squares refer to AESWS data obtained with different CPWs on nominally identical antidot lattices. Full lines are calculated dispersions, where $k_\perp$ is varied, but (a) $k_\parallel = \pi/600$ nm and (c) $k_\parallel = \sqrt{2}\pi/600$ nm (considering $M_s = 760$ kA/m and film thickness 22 nm).

position of eigenmodes of different frequency. Here we have found AESWS to be powerful as it operates frequency resolved. The total amplitude I_{tot} measured at the detector CPW depends on four relevant parameters: (i) the angle-dependent excitation strength of the specific mode [compare the reflection data depicted in Fig. 1(d)]; (ii) the propagation velocity (a large v_g results in a short propagation time t and a high amplitude at the detector); (iii) the characteristic relaxation time τ of the given mode; (iv) the em crosstalk $\tilde{I}$ between the two CPWs. We find $\tilde{I}$ to be almost constant over the relevant frequency range from 4 to 10 GHz. The constant $\tilde{I}$ is eliminated by studying the variation of I_{tot} for different eigenfrequencies and group velocities v_g at different external fields 15 mT $\leq \mu_0 H \leq$ 60 mT. We make use of the intrinsic dependence of v_g on the SW eigenfrequency [8]. Based on such data sets, τ is evaluated from

$$\frac{I}{I_0} = \frac{I_{\text{tot}} - \tilde{I}}{I_0} = \exp\frac{-t}{\tau} = \exp\frac{-s}{v_g \tau}. \qquad (2)$$

Figure 2(d) exemplarily shows fitted curves (solid lines) where we use τ of Eq. (2) as the free parameter to extract the relaxation characteristics of two different AESWS data sets. For the unpatterned plain film one obtains a relaxation time of $\tau = 0.6 \pm 0.1$ ns which, in particular, does not depend on η. This value is consistent with relaxation times reported in the literature which have been extracted by time-resolved experiments [25]. For the antidot lattice one observes angle-dependent relaxation characteristics [full circles in Fig. 1(e)]. At $\eta = 0°$ (regime A) the effective relaxation time is 0.70 ± 0.2 ns, i.e., comparable with the plain film. A minimum relaxation time $\tau = 0.37 \pm 0.1$ ns is found at $\eta = 22°$ (regime B). If compared to regime A, the effective relaxation increases by a factor of almost two in regime B. A larger relaxation time $\tau = 0.49 \pm 0.2$ ns is regained in regime C, but still the value is smaller than τ at $\eta = 0°$ and of the unpatterned film. The relaxation times vary with the characteristic mode profiles illustrated in Figs. 2(a)–2(c). In regime B the propagating mode has a higher oscillation amplitude near the edges of the holes if compared to A and C. Near the hole edges, the internal field can vary due to edge roughness and reduced saturation magnetization through Gallium implantation by focussed ion beam etching. Via magnon-magnon scattering, such irregularities can open further relaxation channels. This might explain the anisotropy of τ found in the angular dependent experiments. However, a theory linking mode profiles and edge roughness with relaxation is missing.

In conclusion we have shown that by removing only a small fraction of about 7% of material from a film to form an antidot lattice, the properties of propagating spin waves are significantly altered. Depending on the orientation of the external field, spin waves are found to propagate at velocities being comparable with or a factor of about two smaller than the velocities found for a plain film. In contrast to the film, the damping characteristics turn out to be highly anisotropic suggesting that extrinsic damping due to, e.g., edge-roughness mediated scattering is relevant in an antidot lattice. Still we find propagation paths on the order of several μm making antidot lattices interesting for spin-wave filtering and field-controlled spin-wave guiding.

*grundler@ph.tum.de

[1] K.-S. Lee, D.-S. Han, and S.-K. Kim, Phys. Rev. Lett. **102**, 127202 (2009).
[2] H. Puszkarski and M. Krawczyk, Solid State Phenom. **94**, 125 (2003).
[3] G. Gubbiotti et al., Appl. Phys. Lett. **90**, 092503 (2007).
[4] J. Topp et al., Phys. Rev. Lett. **104**, 207205 (2010).
[5] S. Neusser and D. Grundler, Adv. Mater. **21**, 2927 (2009).
[6] V. V. Kruglyak, S. O. Demokritov, and D. Grundler, J. Phys. D **43**, 264001 (2010).
[7] G. Gubbiotti et al., J. Phys. D **43**, 264003 (2010).
[8] M. Bailleul, D. Olligs, and C. Fermon, Appl. Phys. Lett. **83**, 972 (2003).
[9] M. Covington, T. M. Crawford, and G. J. Parker, Phys. Rev. Lett. **89**, 237202 (2002).
[10] Z. Liu et al., Phys. Rev. Lett. **98**, 087201 (2007).
[11] K. Perzlmaier, G. Woltersdorf, and C. H. Back, Phys. Rev. B **77**, 054425 (2008).
[12] V. Vlaminck and M. Bailleul, Science **322**, 410 (2008).
[13] V. E. Demidov et al., Appl. Phys. Lett. **92**, 232503 (2008).
[14] V. E. Demidov et al., Phys. Rev. B **79**, 054417 (2009).
[15] K. Vogt et al., Appl. Phys. Lett. **95**, 182508 (2009).
[16] F. Giesen et al., Phys. Rev. B **75**, 184428 (2007).
[17] K. J. Kennewell, M. Kostylev, and R. L. Stamps, J. Appl. Phys. **101**, 09D107 (2007).
[18] S. Neusser, B. Botters, and D. Grundler, Phys. Rev. B **78**, 054406 (2008).
[19] F. Giesen et al., J. Appl. Phys. **97**, 10A712 (2005).
[20] I. Neudecker et al., Phys. Rev. B **73**, 134426 (2006).
[21] D. V. Berkov and N. L. Gorn, Micromagus - software for micromagnetic simulations (2008), http://www.micromagus.de/.
[22] A single unit cell of the antidot lattice with two-dimensional periodic boundary conditions was simulated. A spatially homogeneous field pulse of 8 mT was used to excite spin precession. Parameters were $M_s = 760$ kA/m, film thickness $b = 22$ nm, exchange stiffness $A = 1.3 \times 10^{-9}$ J/m, simulation unit cell size $10 \times 10 \times 22$ nm^3, and damping constant $\alpha = 0.01$.
[23] S. Neusser et al., Appl. Phys. Lett. **93**, 122501 (2008).
[24] B. Kalinikos and A. Slavin, J. Phys. C **19**, 7013 (1986).
[25] T. J. Silva et al., J. Appl. Phys. **85**, 7849 (1999).